



# 1 Diagnosing Dissolved Organic Carbon Simulation of 2 SWAT-C model Using Machine Learning Approaches

3 Zehong Huang<sup>1</sup>, Shouzhi Chen<sup>1</sup>, Yufeng Gong<sup>1</sup>, Zheng Wang<sup>2</sup>, Zheng Duan<sup>3</sup>,  
4 Yongshuo H. Fu<sup>1</sup>

5 <sup>1</sup>College of Water Sciences, Beijing Normal University, Beijing, China

6 <sup>2</sup>College of Urban and Environmental Sciences, Central China Normal University, Wuhan, China

7 <sup>3</sup>Department of Physical Geography and Ecosystem Science, Lund University, Sölvegatan 12, SE-223  
8 62 Lund, Sweden

9 *Correspondence to:* Yongshuo H. Fu (Email: yfu@bnu.edu.cn);

10 **Abstract.** Dissolved organic carbon (DOC) plays a critical role in the terrestrial carbon cycle, and  
11 accurate simulation of its dynamics is essential for understanding carbon balance and climate change  
12 mitigation. However, DOC simulations still involve large uncertainty under complex environmental  
13 conditions. To address this challenge, we proposed a Module Diagnosis Framework (MDF) that  
14 quantitatively identifies the module-level sources of uncertainty in DOC modeling. The SWAT-MDF  
15 integrates the physically based SWAT-Carbon (SWAT-C) model with a data-driven module that  
16 employs machine learning algorithms and applies Shapley additive explanations (SHAP) and residual  
17 analysis to diagnose the uncertain source of DOC simulation in the Yalong River Basin. We found that  
18 the data-driven module based on bidirectional long short-term memory (Bi-LSTM) networks achieved  
19 good performance for daily DOC predictions with an average  $NSE = 0.62$ ,  $R^2 = 0.67$ ,  $KGE = 0.74$  while  
20 the original SWAT-C model yielded average  $NSE = 0.51$  and  $R^2 = 0.61$ ,  $KGE = 0.55$ . Despite this  
21 improvement, the testing performance remains limited, suggesting that the main uncertainty arises from  
22 the structural limitations of SWAT-C and highlighting the need for further structural improvement and  
23 module-level diagnosis. The MDF results revealed that the carbon cycle module and pollutant transport  
24 module mainly regulated the magnitude and variation of DOC predictions in the original SWAT-C  
25 model, and the vegetation growth module and the carbon cycle module were major sources of DOC  
26 prediction uncertainties. We therefore proposed that further improvements in DOC prediction in the  
27 SWAT-C model should focus on the vegetation growth, carbon cycle modules. Our proposed  
28 SWAT-MDF framework significantly enhances the reliability of DOC simulations, and provides a



29 quantitative basis for improving the SWAT-C model and offers a generalizable approach to module  
30 optimization in similar coupled modeling frameworks.  
31



## 32 **1 Introduction**

33 Dissolved organic carbon (DOC) is a critical component of the terrestrial carbon-water cycle and  
34 constitutes the primary form of carbon exported from watersheds to stream and river system (Evans et  
35 al., 2005). It accounts for over 50% of the total terrestrial organic carbon flux entering the oceans (Cole  
36 et al., 2007), underscoring its importance in the global carbon cycle. The dynamic behavior of DOC is  
37 closely linked to substantial changes in terrestrial carbon storage. Although DOC is not considered a  
38 pollutant itself, its excessive presence can facilitate the co-transport of toxic substances such as heavy  
39 metals through complexation processes, thereby adversely affecting surface water quality (Harkort and  
40 Duan, 2023; Lawlor and Tipping, 2003). Consequently, accurately quantifying DOC dynamics is  
41 essential for understanding carbon input and output processes at the watershed scale and provides  
42 crucial data support for pollution policy-making and climate change adaptation (Du et al., 2023).

43 Currently, watershed-scale DOC monitoring predominantly relies on water-quality sampling.  
44 However, the limited spatial distribution of fixed monitoring stations and the lack of long-term  
45 observational data hinder comprehensive characterization of DOC's spatiotemporal variability (Wang  
46 et al., 2025). As a result, physically-based modeling approaches have become indispensable tools in  
47 DOC studies. Among these, the Soil and Water Assessment Tool (SWAT) has been widely utilized to  
48 simulate hydrological and water quality dynamics under various land-use and climate change scenarios  
49 (Srinivasan et al., 1998). Yang and Zhang, (2016) developed a carbon cycling module for SWAT  
50 (Zhang et al., 2013), while Du et al., (2019) extended this framework by incorporating updated  
51 algorithms to simulate DOC transport and transformation processes (Qi et al., 2020b). The enhanced  
52 SWAT-C model has demonstrated promising potential for watershed-scale DOC simulation, yielding  
53 relatively accurate results in diverse basins, such as forested watersheds (Lee et al., 2025) and  
54 agricultural watersheds (Qi et al., 2020a). However, when the model is applied to new regions, it still  
55 faces considerable challenges. The pronounced heterogeneity in land use, topography, and climatic  
56 conditions across watersheds necessitates parameter regionalization. Nevertheless, the characterization  
57 of watershed features during regionalization remains insufficiently defined (Liu et al., 2024; Razavi  
58 and Coulibaly, 2013) which can lead to reduced model performance. This is particularly evident under



59 complex environmental conditions where SWAT-C model tends to underestimate high flows and DOC  
60 peak fluxes (Qi et al., 2020a). In addition, incomplete module designs and vague parameter  
61 representations exacerbate prediction uncertainties. Existing studies have rarely conducted quantitative,  
62 module-level diagnosis; instead, they typically rely on subjective model adjustments, which may lead  
63 to inconsistent calibration and unreliable results..

64 Therefore, developing quantitative module diagnosis frameworks is essential to identify and  
65 improve critical sub-modules affecting DOC prediction, thereby enhancing the robustness and  
66 generalizability of the coupled modeling approach.

67 In recent years, machine learning (ML) has demonstrated substantial potential in hydrological  
68 modeling, particularly for capturing complex nonlinear interactions among variables (Fan et al., 2020).  
69 As data-driven tools, ML models can autonomously learn latent relationships without requiring  
70 extensive prior knowledge, and they often outperform traditional process-based models in terms of  
71 simulation accuracy, generalizability, and robustness (Lee et al., 2023a; Yao et al., 2023). However, the  
72 “black-box” nature of ML models limits their interpretability, raising concerns in environmental  
73 decision-making and policy implementation contexts (Carvalho et al., 2019). To address the  
74 performance limitations of physically-based models under complex environmental conditions and the  
75 limited interpretability of ML approaches, hybrid modeling frameworks have been proposed. Recent  
76 studies have integrated hydrological and machine learning models to explore the dominant factors  
77 influencing streamflow variability, demonstrating the advantages of combining physical-based and  
78 data-driven approaches in hydrological modeling (Ding et al., 2025). In addition, a SWAT-ELM-SHAP  
79 hybrid modeling framework has been proposed to improve both predictive accuracy and interpretability  
80 of blue and green water simulations in data-scarce watersheds by incorporating ensemble learning and  
81 model explainability techniques (Guo et al., 2024). In this framework, the Extreme Learning Machine  
82 (ELM), a single-layer feedforward neural network known for its fast training speed, is used to predict  
83 blue and green water components. Shapley additive explanations (SHAP) are applied to interpret  
84 feature contributions, thereby enhancing model transparency.

85 Despite recent advancements, accurate simulation of DOC remains challenging due to the  
86 complexity of watershed environmental conditions, limited long-term monitoring data, and

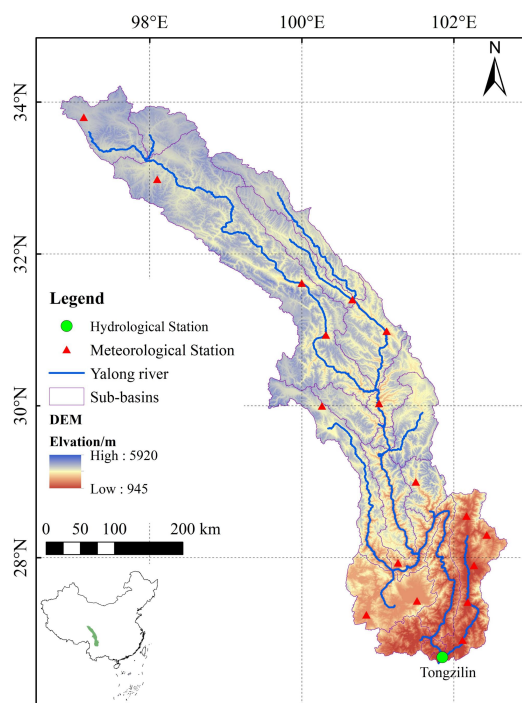


87 inadequately developed model modules. The SWAT-MDF quantitatively diagnoses module-level  
88 sources of uncertainty in SWAT-C and evaluates their relative contributions under complex  
89 environmental conditions. To support this diagnostic process, the data-driven module compares eight  
90 algorithms to identify the optimal approach for reproducing the nonlinear dynamics of DOC.  
91 Subsequently, Shapley Additive Explanations (SHAP) and residual analysis are applied to interpret this  
92 representation, quantify feature and module contributions, and pinpoint sub-modules that dominate  
93 simulation uncertainty (Lundberg et al., 2020). The main objective of this study is to establish a  
94 quantitative diagnosis of module-level uncertainties in DOC simulations using the SWAT-MDF  
95 framework and to provide a scientific basis for targeted model refinement.

## 96 **2. Materials and methods**

### 97 **2.1. Study area**

98 The Yalong River Basin, located in Southwest China (Fig. 1), is the largest tributary of the Jinsha  
99 River, which constitutes the upper reaches of the Yangtze River. Originating from the southern slopes  
100 of the Bayan Har Mountains on the Qinghai Tibet Plateau, the river traverses Qinghai Province,  
101 Sichuan Province, and the Tibet Autonomous Region. Geographically, the basin extends from 96°52' to  
102 102°48'E and 26°32' to 33°58'N, spanning approximately 1,571 km in length and covering an area of  
103 about 136,000 km<sup>2</sup>. The basin features highly variable terrain, with an average elevation exceeding  
104 3,000 meters (Liu et al., 2019).



105  
 106 **Figure 1.** Overview of the Yalong River Basin. The inset at the lower left shows the basin's location within China.

107       The average annual runoff of the basin is 1,914 m<sup>3</sup>/s, and the average annual export of suspended  
 108 particulate matter reaches approximately 2.55\*10<sup>10</sup> kg. Precipitation varies significantly across  
 109 regions—ranging from 500-800 mm in the headwaters to 900-1,300 mm in the lower reaches, with  
 110 certain midstream areas receiving as much as 1,000-1,800 mm annually (Li et al., 2014). Influenced by  
 111 the monsoon climate, the basin experiences distinct seasonal hydrological variation: the wet season  
 112 spans from May to October, characterized by concentrated rainfall and runoff with pronounced river  
 113 flow fluctuations; the dry season occurs from November to April, with markedly reduced runoff.  
 114 Additionally, snowmelt contributes to runoff between March and June each year, supplementing  
 115 rainfall inputs (Zhao et al., 2021). In this study, the Tongzilin Hydrological Station, located in the lower  
 116 reaches of the Yalong River, was selected for analysis. Its runoff, sediment, and DOC monitoring data  
 117 are highly representative and reliable, providing robust support for the investigation of hydrological  
 118 processes, DOC dynamics, and model optimization in the basin.



## 2.2. Data source

The SWAT-C model developed in this study was constructed using a suite of input datasets, including meteorological, topographic, soil, and land use information, as summarized in Tab. 1. Meteorological data spanning from 1970 to 2020, including precipitation, relative humidity, maximum and minimum air temperature, solar radiation and wind speed, were obtained from eleven stations (Tab. 1) archived by the China Meteorological Data Service Center. Model calibration and validation were performed using observed runoff, sediment, and DOC data. Daily runoff and sediment observations at the Tongzilin Hydrological Station in the Yalong River Basin for the period 2013-2020 were sourced from the Hydrological Yearbook of the People's Republic of China. DOC observations for 2013-2014 and 2019-2020 were derived from field measurements conducted by Xu et al., (2024) at the same station. Description of DEM, soil data and land use map.

**Table 1 .Data Sources for the study.**

Data Type	Description	Source
Meteorological	Daily station-based	China Meteorological Data Service Center ( <a href="https://data.cma.cn/">https://data.cma.cn/</a> )
DEM	ASTER GDEM 30M	Geospatial Data Cloud ( <a href="https://www.gscloud.cn/">https://www.gscloud.cn/</a> )
Soil Data	HWSD Global Soil Database	Institute of Soil Science, Chinese Academy of Sciences ( <a href="http://english.issas.cas.cn/">http://english.issas.cas.cn/</a> )
Land Use Map	2014 land use distribution	CLCD dataset, Wuhan University ( <a href="http://doi.org/10.5281/zenodo.4417809">http://doi.org/10.5281/zenodo.4417809</a> )
Runoff Data	Daily observations	Hydrological Yearbook of the People's Republic of China
Sediment Data	Daily observations	Hydrological Yearbook of the People's Republic of China
DOC Data	Daily observations	Escalating Carbon Export from High-Elevation Rivers in a Warming Climate (Xu et al., 2024)

## 2.3. The SWAT-MDF Coupled Modeling Framework

The SWAT-MDF diagnostic framework developed in this study quantitatively identifies and interprets the module-level sources of uncertainty in DOC simulations. It integrates three main components (Fig. 2): the SWAT-C model, a data-driven module, and a module diagnosis framework based on SHAP and residual analysis. These components are connected in a sequential structure, in



136 which outputs from each stage serve as inputs for the subsequent stage, enabling a complete workflow  
137 encompassing initial simulation, data-driven module, and comprehensive module diagnosis.  
138 Specifically, multiple calibrated SWAT-C outputs (feature parameters) are treated as diagnostic  
139 variables that help trace uncertainty propagation through the coupled system. Subsequently, SHAP  
140 interpretation and residual analysis are applied to the data-driven results to quantify the contributions of  
141 different SWAT-C modules and identify the dominant sources of structural uncertainty within the  
142 model.

143 The first component (Fig. 2a), SWAT-C model, provides the physical and mechanistic foundation  
144 of the diagnostic framework (Section 2.3.1). Its simulations are driven by spatial datasets such as  
145 digital elevation model (DEM), soil type, land use and slope, as well as meteorological variables  
146 including precipitation, relative humidity, maximum and minimum temperature, wind speed and solar  
147 radiation. Upon model calibration (More details are provided in Text S1 in the Supplementary  
148 Materials.), a subset of key characteristic parameters that govern DOC dynamics within the watershed  
149 was identified. These parameters, each linked to specific physical modules in the SWAT-C structure,  
150 are used as feature inputs for the second component of the framework. Tab. 2 provides detailed  
151 definitions of these parameters and their associated modules within SWAT-C model.

152 The second component (Fig. 2b) is a data-driven module that establishes nonlinear relationships  
153 between SWAT-C simulations and observed DOC data to support subsequent diagnostic analysis. In  
154 this module, several ML algorithms are employed to learn process-dependent relationships and  
155 generate data representations for interpretability analysis in the next stage. Eight ML algorithms were  
156 implemented (Section 2.3.2): convolutional neural network (CNN), support vector regression (SVR),  
157 extreme gradient boosting (XGBOOST), multilayer perceptron (MLP), and four variants of long  
158 short-term memory (LSTM)—vanilla LSTM (V-LSTM), bidirectional LSTM (Bi-LSTM), stacked  
159 LSTM (St-LSTM), and convolutional LSTM (Cv-LSTM)(More details are provided in Texts S2 and S3  
160 in the Supplementary Materials.). A transfer learning strategy was implemented, wherein the models  
161 were initially pretrained using long-term simulation outputs from SWAT-C model and subsequently  
162 fine-tuned with observed DOC data. Bayesian optimization was applied to ensure model robustness  
163 and stability for the subsequent SHAP-based and residual analyses.



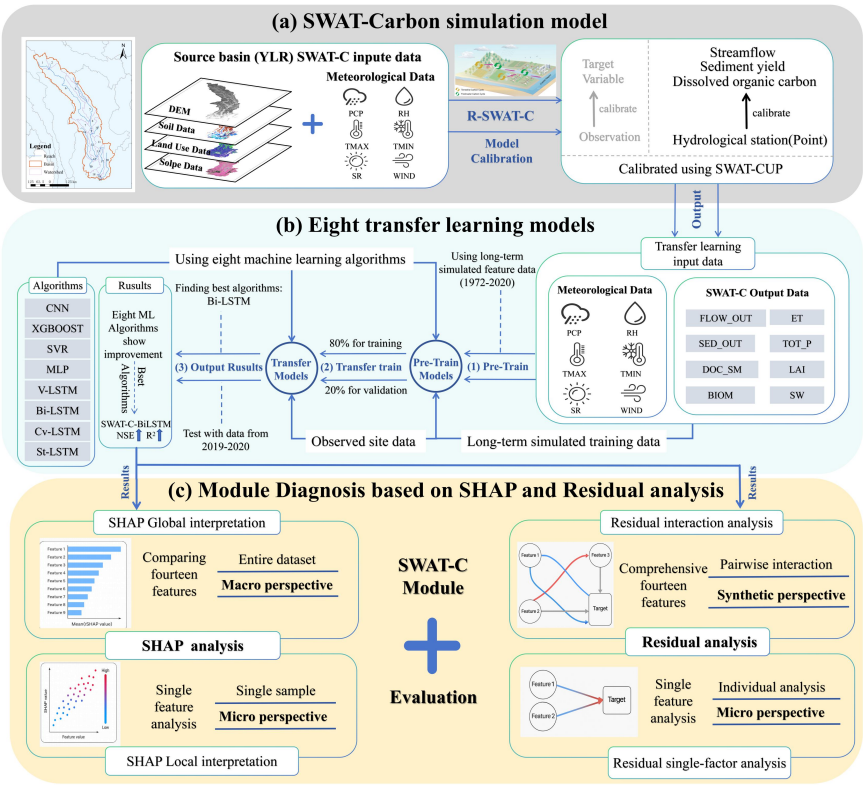


**Figure 2.** The SWAT-MDF Coupled Model Technical Framework. The computational and diagnosis procedures are illustrated from top to bottom: (a) SWAT-Carbon simulation module; (b) Data-driven model; (c) Module diagnosis Using SHAP and Residual Analysis.

The third component (Fig. 2c) diagnosis SWAT-C modules using SHAP interpretation and residual analysis (Section 2.3.3). SHAP quantifies both global and local contributions of input features, improving model interpretability. The residual contribution rate is employed to measure each module's relative share of total prediction error, providing an objective comparison of module reliability. By combining SHAP-based feature attribution with residual decomposition, the SWAT-MDF framework pinpoints modules that dominate structural uncertainty and provides a quantitative basis for targeted model refinement. This diagnostic approach shifts the analytical focus from empirical calibration toward mechanistic understanding and structural evaluation of process-based DOC simulations.

**Table 2.** SWAT-C model Feature Parameters

Data Name	Definition	SWAT-C Module
-----------	------------	---------------



FLOW_OUT	Streamflow output	Runoff module
SED_OUT	Sediment output	Sediment module
DOC_Simulate	Simulated total DOC	Carbon cycle module
BIOM	Biomass	Biomass module
ET	Evapotranspiration	Evapotranspiration module
TOT_P	Total phosphorus output	Pollutant transport module
LAI	Leaf area index	Vegetation growth module
SW	Soil water content	Soil moisture module
PCP, RH, TMAX, TMIN, SR, WIND	Precipitation, Relative humidity, Max/Min Temperature, Solar radiation, Wind speed	Meteorological forcing module

177 Note: The specific locations of the SWAT-C modules in the source code are provided in Table S4 in the  
178 Supplementary Materials. All feature parameters were derived from the calibrated SWAT-C model.

### 179 2.3.1. SWAT-C Model

180 The SWAT is a physically based, semi-distributed hydrological model capable of continuous  
181 simulation. It has been extensively applied in watershed-scale hydrology and water quality studies for  
182 replicating the rainfall–runoff process (Rathjens et al., 2015; Srinivasan et al., 1998). By incorporating  
183 multi-source inputs such as climate, soil, and land use data, SWAT provides a robust platform for  
184 quantitatively assessing the impacts of climate change and anthropogenic activities on watershed  
185 hydrology and environmental conditions (Tan et al., 2019).

186 In the SWAT-MDF coupled modeling framework, we adopted an enhanced version of SWAT  
187 known as SWAT-C, which integrates the CENTURY biogeochemical model to enable dynamic  
188 simulation of soil organic matter and carbon processes (Zhang et al., 2013). Yang and Zhang (2016)  
189 demonstrated the model's reliability for simulating key forest ecosystem variables, such as  
190 evapotranspiration and net primary productivity. Building on this, Du et al., (2019) expanded the  
191 model's functionality to couple terrestrial and aquatic carbon cycling, facilitating watershed-scale  
192 simulation of DOC transport. The current SWAT-C model, built upon the SWAT2012 framework, has  
193 demonstrated strong simulation performance in snowmelt-dominated basins (Grusson et al., 2015).



194 Through the innovative integration of core algorithms from water quality models such as QUAL2K and  
 195 CE-QUAL-W2 (Pelletier et al., 2006), SWAT-C has established a comprehensive carbon cycle  
 196 simulation system. This system includes modules for soil-derived dissolved organic carbon (DOC)  
 197 generation and transport, as well as the biogeochemical cycling of DOC within river channels (Lee et  
 198 al., 2025). A full description of the spatial setup and parameterization is provided in Text S1 in the  
 199 Supplementary Materials.

### 200 **2.3.2. Data-driven Models**

201 The data-driven component of the SWAT-MDF framework is implemented through a set of  
 202 machine learning (ML) models. ML methods, characterized by data-driven modeling strategies,  
 203 circumvent the dependence of traditional hydrological models on subjective prior knowledge. Their  
 204 strong capacity for nonlinear fitting has introduced a new paradigm for hydrological simulations (Lee  
 205 et al., 2023b; Todini, 2007). To address DOC simulation requirements in the Yalong River Basin, this  
 206 study reviewed and compared commonly used ML approaches in hydrological contexts, see Text S2 in  
 207 the Supplementary Materials. Eight ML methods were ultimately selected for the data-driven module:  
 208 CNN, SVR, XGBOOST, MLP, and four LSTM variants, including V-LSTM, St-LSTM, Bi-LSTM, and  
 209 Cv-LSTM.

210 DOC observations from 2013-2014 were used as training data, with 20% randomly withheld for  
 211 validation, while observations from 2019-2020 were used for testing. Given the limited availability of  
 212 DOC measurements, a transfer learning strategy was adopted. First, models were pretrained on  
 213 long-term simulated feature parameters from the SWAT-C model (1972-2020) to establish fundamental  
 214 relationships between inputs and DOC outputs. Second, the pretrained models were fine-tuned using  
 215 observed data to better match the true data distribution. This process mitigated overfitting caused by  
 216 data scarcity by leveraging generalized patterns learned from simulations. Text S3 in the  
 217 Supplementary Materials details the principles of the selected ML methods and the procedures for  
 218 Bayesian-based hyperparameter optimization.

### 219 **2.3.3. Calibration and Module Diagnosis of the Coupled Model**

220 This study conducted preliminary simulations of runoff, sediment, and DOC in the Yalong River



221 Basin using the SWAT-C model. Daily outputs were calibrated and validated using DOC observations  
 222 from 2013 to 2020, together with runoff and sediment data from the Tongzilin Station. The DOC  
 223 calibration (2013-2014) and validation (2019-2020) periods included 34 and 38 samples, respectively,  
 224 with consistent periods applied to runoff sediment. Model performance was evaluated using the  
 225 Nash-Sutcliffe efficiency (*NSE*), coefficient of determination ( $R^2$ ) and Kling-Gupta efficiency (*KGE*).  
 226 Model parameters were automatically calibrated using the SUFI-2 algorithm in SWAT-CUP  
 227 (Abbaspour et al., 2017). Detailed parameter values and sensitivity analysis results are presented in  
 228 Text S1 in the Supplementary Materials.

229 To interpret DOC predictions from the coupled model, SHAP was employed. Rooted in  
 230 cooperative game theory, SHAP considers each input feature as a contributor, with the SHAP value  
 231 quantifying the marginal contribution of a feature to a specific prediction (Lundberg et al., 2020). Two  
 232 strategies were adopted: (1) global interpretation, using the mean SHAP values across all samples to  
 233 rank feature importance; (2) local interpretation, evaluating the SHAP values for individual predictions  
 234 to determine the direction and magnitude of each feature's influence.

235 Residuals, which are defined as the differences between predicted and observed values, were  
 236 further analyzed to assess the model bias and predictive uncertainty. To quantify the influence of input  
 237 features on prediction errors, residuals were computed for each sample, and polynomial feature  
 238 expansion was applied to generate nonlinear interaction terms. Ridge regression was subsequently used  
 239 to explore the relationship between these terms and the residuals (Santos Nobre and Da Motta Singer,  
 240 2007; Tyagi et al., 2022). The absolute values of the regression coefficients served as indicators of each  
 241 feature's contribution to the residuals (Eq. 1). This allowed for the quantification of both individual  
 242 feature effects and interaction-driven contributions to model errors. To evaluate the robustness of these  
 243 estimates, a bootstrapping approach was used to repeatedly resample the training dataset (Hongyi Li  
 244 and Maddala, 1996), and the mean and standard deviation of each feature's contribution rate were  
 245 computed to characterize uncertainty. Two residual analysis strategies were adopted: (1)  
 246 Interaction-based: capturing nonlinear feature interactions via polynomial expansion and ridge  
 247 regression; (2) Single-feature: assessing individual feature contributions without interactions.



$$C_j = \frac{|\beta_j|}{\sum_{i=1}^n |\beta_i|} \times 100\% \quad (1)$$

where  $C_j$  denotes the contribution rate of the  $j$ -th feature to the residuals, expressed as a percentage;  $\beta_j$  denotes the ridge regression coefficient corresponding to the  $j$ -th feature;  $n$  denotes the total number of input features.

### 3. Results

#### 3.1. Model performance of SWAT-C Model in DOC simulations

The first component of the coupled model, the SWAT-C model, achieved excellent performance in simulating daily runoff and sediment for the Yalong River Basin (Fig. 3). During the calibration period, the SWAT-C model achieved high accuracy for daily runoff (calibration:  $NSE = 0.91$ ,  $R^2 = 0.92$ ,  $KGE = 0.94$ ; validation:  $NSE = 0.90$ ,  $R^2 = 0.93$ ,  $KGE = 0.85$ ). For sediment, both calibration and validation phases yielded excellent results (calibration:  $NSE = 0.92$ ,  $R^2 = 0.92$ ,  $KGE = 0.95$ ; validation:  $NSE = 0.89$ ,  $R^2 = 0.93$ ,  $KGE = 0.79$ ). In contrast, the model's ability to simulate daily DOC was relatively limited, with lower performance (calibration:  $NSE = 0.59$ ,  $R^2 = 0.59$ ,  $KGE = 0.70$ ; validation:  $NSE = 0.42$ ,  $R^2 = 0.63$ ,  $KGE = 0.40$ ). Specifically, the model consistently overestimated DOC concentrations during both high-flow and low-flow periods, resulting in an overall positive bias. Additionally, the simulated seasonal pattern showed a slight temporal mismatch, with peak DOC concentrations in some times occurring later than observed.

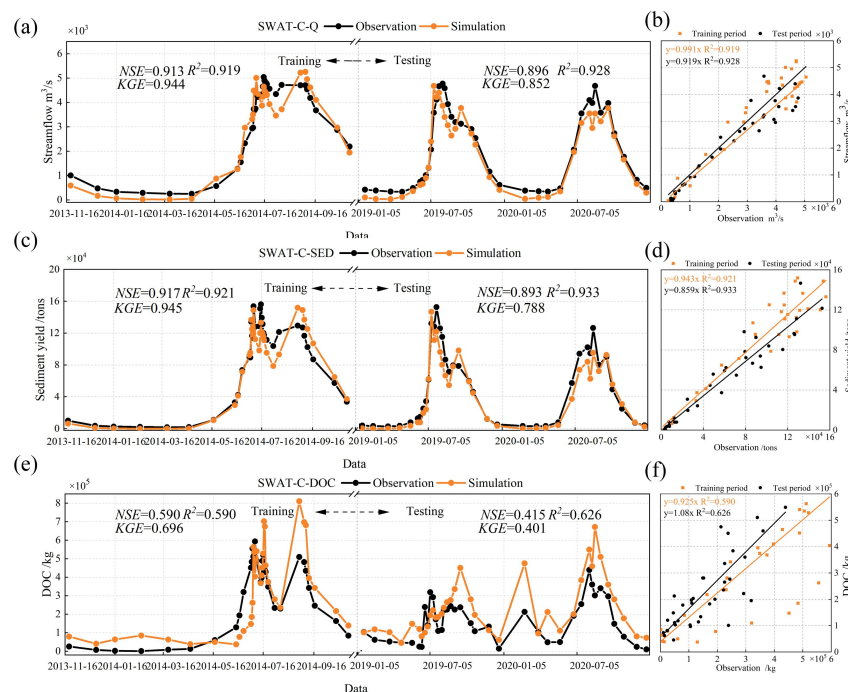


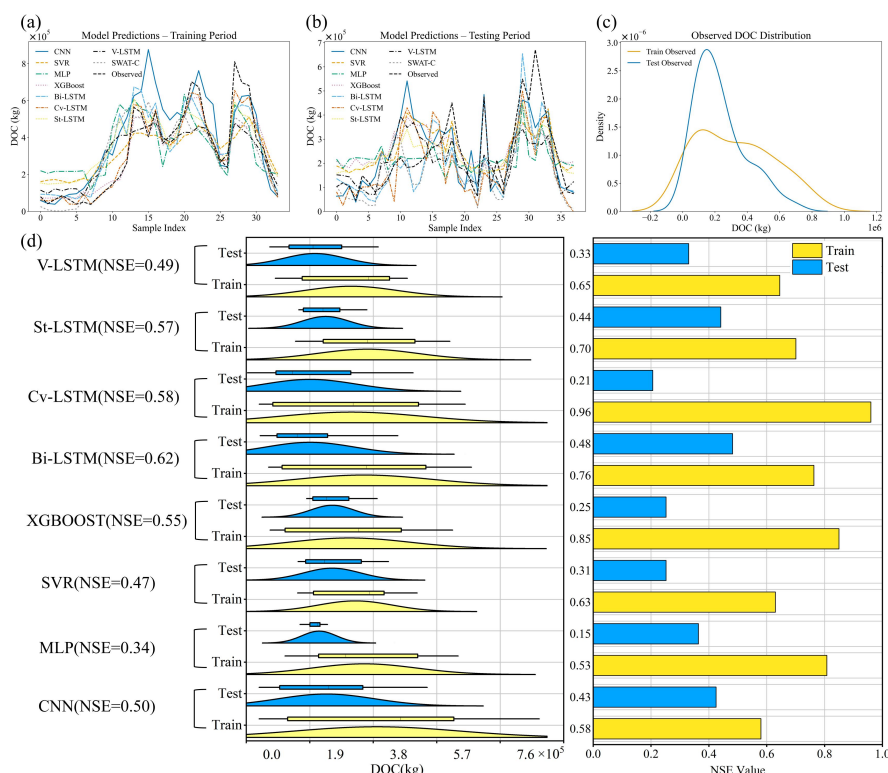
**Figure 3.** Simulation performance of the SWAT-C model. Line plots (a) streamflow (Q), (c) sediment yield (SED), and (e) dissolved organic carbon (DOC). Scatter plots (b), (d), and (f) show the correlations between observed and simulated values.

### 3.2. Comparison of Data-driven Module Performance

The performance of the data-driven module in the SWAT-MDF framework was evaluated using eight algorithms to simulate daily DOC dynamics (Fig. 4d). Among these, the Bi-LSTM based data-driven model achieved the best performance (training:  $NSE = 0.76$ ,  $R^2 = 0.78$ ,  $KGE = 0.80$ , testing:  $NSE = 0.48$ ,  $R^2 = 0.55$ ,  $KGE = 0.67$ ). With the exception of MLP and CNN, most algorithms reproduced DOC variations more effectively than the calibrated SWAT-C model (training:  $NSE = 0.59$ ,  $R^2 = 0.59$ ,  $KGE = 0.70$ , testing:  $NSE = 0.42$ ,  $R^2 = 0.63$ ,  $KGE = 0.40$ ), though the degree of improvement varied among methods. Violin plots of DOC predictions, together with NSE analysis, indicate that St-LSTM and Bi-LSTM exhibit minimal differences between the training and testing phases, demonstrating relatively strong generalization, robustness, and model stability. In contrast, although XGBOOST, MLP, and SVR performed well during training, they exhibited significant biases



280 and notable drops in performance on the test set. Notably, the Bi-LSTM model effectively captured  
 281 both short- and long-term dependencies in the data, enabling better simulation of the complex  
 282 nonlinear dynamics of DOC.



283  
 284 **Figure 4.** Performance comparison of eight algorithms in DOC prediction. (a) and (b) present time series plots of  
 285 simulated versus observed DOC values during the training and testing periods, respectively. (c) shows the kernel  
 286 density estimation of observed DOC distributions for both datasets. (d) compares model-specific distributions of  
 287 predicted DOC using violin plots (left), alongside their corresponding NSE values (right) for both training and  
 288 testing periods.

289 The results of the SWAT-MDF-BiLSTM model highlights the advantage of using physically based  
 290 features derived from SWAT-C. These features helped the Bi-LSTM model capture key watershed  
 291 processes and learn complex relationships between input variables and DOC output. Although the  
 292 integration improved the model's predictive ability, the testing results were still limited, suggesting the  
 293 model struggles to fully capture DOC dynamics. This finding underscores the necessity of subsequent  
 294 module-level diagnosis within the SWAT-MDF framework to identify and address these structural



295 limitations. Overall, the integration of data-driven modeling with process-based information provides a  
296 reliable foundation for uncertainty attribution and module diagnosis in complex watershed systems.

### 297 **3.3. SHAP and Residual-Based Model Diagnosis**

#### 298 **3.3.1. Global Interpretation of Input Features**

299 Based on the comparison of Data-driven Module Performance in Section 3.2, the  
300 SWAT-MDF-BiLSTM model, which demonstrated the highest performance, was selected for further  
301 analysis. In this coupled framework, global SHAP interpretation was employed to identify the most  
302 influential input features contributing to DOC prediction. Fig. 5 illustrates the global feature  
303 importance ranked by the mean absolute SHAP values. This analysis facilitated the identification of  
304 dominant hydrological and ecological modules driving DOC simulation and provided insights into how  
305 the coupled model captures DOC dynamics within the watershed.

306 Features with a global importance greater than 5% were defined as key contributors. According to  
307 the results (Fig. 5), DOC\_Simulate, TOT\_P, and PRE were identified as the top three features,  
308 accounting for 59.34%, 8.78%, and 6.56% of the total importance, respectively, while other features  
309 exhibited relatively low contributions. DOC\_Simulate corresponds to the Carbon cycle module, which  
310 governs carbon inputs, transformations, cycling, and export-directly shaping DOC behavior. As such, it  
311 exerted a substantially stronger influence than other modules. TOT\_P reflects the pollutant transport  
312 module, which represents the effects of pollution sources on water quality and influences DOC  
313 dynamics through pollutant loading and mixing processes. PRE denotes precipitation, which regulates  
314 runoff generation, soil water content, and evapotranspiration, thereby modifying DOC transport and  
315 concentration across the watershed.



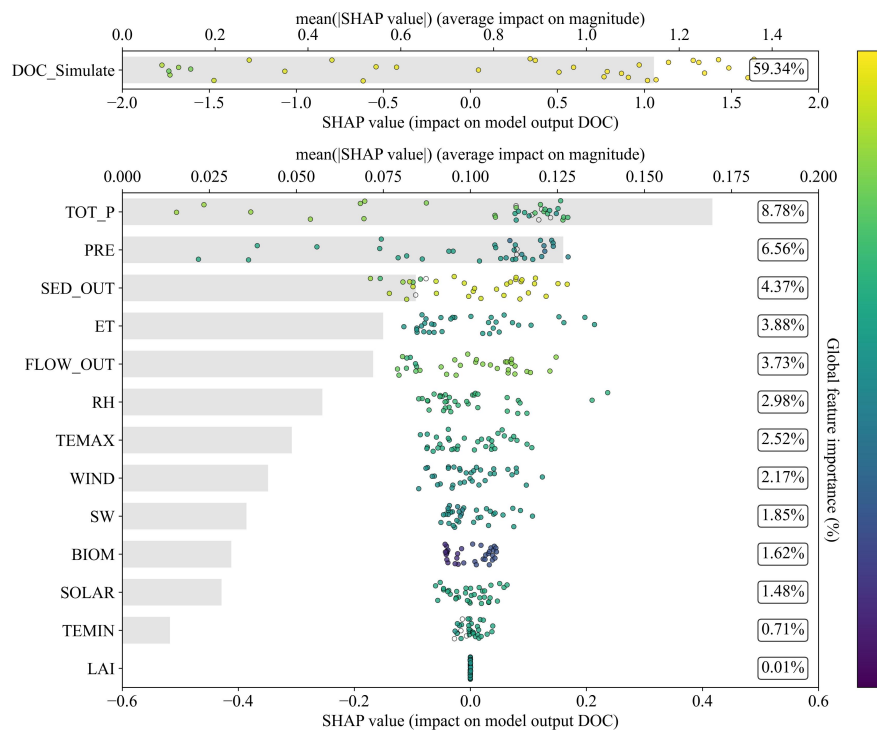
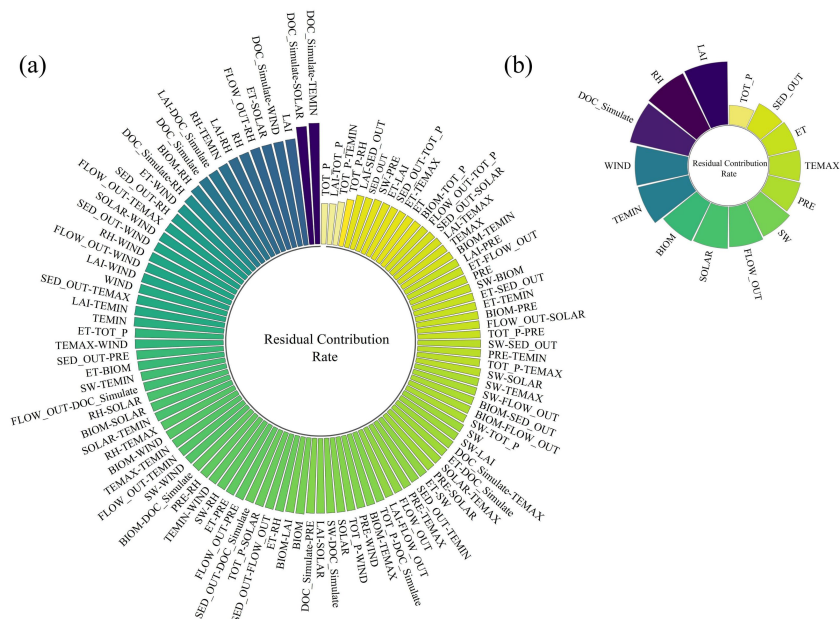


**Figure 5.** Global SHAP analysis of feature parameters. The upper plot shows the distribution of SHAP values for simulated DOC and its impact on the model's DOC predictions. The lower plot illustrates the distribution of SHAP values for input features along with their average impact on DOC prediction.

### 3.3.2. Residual Analysis of Input Features

Residual analysis was further conducted to quantify the contribution of input features to DOC prediction residuals within the coupled model. The five interaction terms with the highest contributions were identified as key factors. As illustrated in the residual interaction analysis (Fig. 6a), the dominant contributors were DOC\_Simulate-TMIN, DOC\_Simulate-SOLAR, LAI, DOC\_Simulate-WIND, and ET-SOLAR, with contribution rates of 2.94%, 2.72%, 1.99%, 1.96%, and 1.95%, respectively. Notably, three of these interactions involved DOC\_Simulate, implying that other environmental variables influence DOC output primarily through their interaction with the carbon cycle simulation module. Additionally, LAI emerged as a major individual contributor, highlighting the significant influence of the vegetation growth module on model residuals.



330  
331 **Figure 6.** Residual analysis of characteristic parameters. (a) presents the detailed contribution rates for all  
332 parameter interactions, while (b) summarizes the primary individual contributions of key parameters. Circular bar  
333 plots illustrating the residual contribution rates of input parameters and their pairwise interactions influencing  
334 model DOC predictions.

335 For individual features, the top three contributors to residual variance were identified as key  
336 single-factor drivers. As shown in the single-feature residual analysis (Fig. 6b), LAI, RH, and  
337 DOC\_Simulate contributed 14.65%, 14.01%, and 13.05%, respectively. LAI represents the vegetation  
338 growth module, which regulates DOC production via its control over plant growth, carbon fixation, and  
339 organic matter input. RH reflects relative humidity, which influences DOC levels indirectly by  
340 affecting vegetation activity, soil water content, and the decomposition of organic material.

341 **3.3.3. Comprehensive Diagnosis of Module Performance**

342 By integrating the results from global SHAP analysis and residual analysis, we identified the key  
343 factors influencing DOC simulation and conducted a comprehensive diagnosis of module performance.

344 The carbon cycle module, represented by DOC\_Simulate, was identified as a dominant factor in  
345 both SHAP and residual analyses. This highlights its central role in DOC simulation and suggests that



errors within this module are a major source of DOC prediction uncertainty. Therefore, targeted improvement of the carbon module is essential to enhance the performance of DOC simulations in SWAT-C model. The pollutant transport module, reflected by TOT\_P, exhibited high global importance in SHAP analysis but contributed little to residuals, indicating relatively stable performance in the DOC simulation process. Similarly, PRE was recognized as a key driver in SHAP analysis but had limited residual influence, suggesting that rainfall data were sufficiently accurate and contributed reliably to the DOC simulation.

The vegetation growth module, indicated by LAI, showed low importance in the global SHAP analysis yet emerged as a major factor in the residual analysis. To investigate this discrepancy, a single-feature SHAP analysis was conducted for LAI (Text S4 in the Supplementary Materials), revealing a negative effect on model output. Given LAI's relatively low temporal variability and stable contribution over time, its global SHAP importance remained limited. However, the high residuals associated with LAI suggest structural issues in the vegetation growth module, indicating a need for further refinement to improve the accuracy of DOC simulations.

Likewise, RH, while showing limited global SHAP importance, appeared as a key factor in the residual analysis. A single-feature SHAP analysis of RH (Text S4 in the Supplementary Materials) indicated a negative impact on DOC prediction. Although RH exhibited considerable temporal variability, its limited global contribution and substantial residual influence imply that RH likely affects DOC outcomes indirectly by influencing other modules. As such, improving the quality and integration of RH data should be prioritized to reduce prediction error in DOC simulations.

## **4. Discussion**

### **4.1. Advantages of Coupling SWAT-C with Data-driven Learning**

Machine learning (ML) models, as a core approach to data-driven learning, exhibit strong capabilities in capturing complex nonlinear patterns from large datasets and are particularly effective in modeling long-term temporal variability. However, they often lack interpretability and struggle to clearly explain how input variables interact to produce outputs (Azzam et al., 2022). In contrast, process-based models such as SWAT-C model offer explicit representations of physical mechanisms



373 and temporal dynamics but tend to underperform in data-scarce or environmentally complex basins due  
374 to limitations in structural completeness and parameter uncertainty (Zhao et al., 2024).

375 Integrating data-driven learning with the process-based SWAT-C model allows these two  
376 paradigms to complement each other. In the SWAT-MDF framework, SWAT-C model provides a rich  
377 set of physically meaningful feature parameters, which serve as external representations of internal  
378 watershed dynamics. These parameters offer valuable physical context for data-driven learning. The  
379 ML component, as the core of this data-driven module, learns the nonlinear relationships between these  
380 parameters and DOC outputs, enabling reliable and effective simulation of DOC under complex  
381 hydrological and environmental conditions. Essentially, this hybrid framework reflects a data-driven  
382 approach grounded in explicit physical processes, establishing a robust foundation for understanding  
383 DOC generation and transport mechanisms.

384 Comparative analysis of eight data-driven algorithms demonstrated that LSTM-based models,  
385 particularly Bi-LSTM, achieved the best performance. This can be attributed to Bi-LSTM ability to  
386 incorporate both past and future information in a time series, allowing it to better capture long-term  
387 dependencies and improve predictive accuracy. Additionally, Bi-LSTM demonstrated superior  
388 performance in modeling nonlinear and highly variable DOC time series, effectively extracting relevant  
389 patterns from complex feature inputs (Siami-Namini et al., 2019). In contrast, models such as  
390 XGBOOST, MLP, and SVR performed reasonably well on the training set but exhibited substantial  
391 performance degradation on the test set. This decline likely reflects the difficulty of traditional ML  
392 models in capturing long-term temporal dependencies and complex nonlinearities, resulting in reduced  
393 generalizability during testing (Zoremsanga and Hussain, 2024).

#### 394 **4.2. Advantages of Using SHAP and Residual Analysis for Module Diagnosis**

395 To enhance the interpretability and diagnostic capacity of the coupled modeling framework, this  
396 study incorporates SHAP and residual analysis as two complementary approaches for module diagnosis.  
397 SHAP quantifies the contribution of each input variable to the predicted DOC outputs, thereby  
398 revealing the internal decision logic of the ML model (Mosca et al., 2022). Its ability to provide both  
399 global and local interpretability makes it particularly effective for identifying key drivers in



400 watershed-scale DOC simulations. In contrast, residual analysis focuses on the discrepancies between  
401 predicted and observed values, facilitating the detection of systematic biases in model outputs (Hantush  
402 and Kalin, 2008). More importantly, when residuals are decomposed by module or variable, they can  
403 reveal the specific contributions of individual sub-modules to the overall simulation error in the  
404 process-based model.

405       These two approaches offer complementary interpretive perspectives. SHAP highlights how input  
406 features influence model outputs, allowing the identification of dominant predictors and enhancing  
407 model transparency. Residual analysis, by quantifying and characterizing prediction errors, links these  
408 errors to specific model components and reveals structural deficiencies. The complementarity between  
409 these methods makes their integration a powerful strategy for achieving both interpretability and  
410 diagnostic insight. Together, they provide a comprehensive framework for module diagnosis that  
411 attributes output behavior to input drivers while diagnosing errors at the module level. In this study, the  
412 integrated framework successfully identified the dominant contribution and error source of the carbon  
413 module in DOC simulation, offering clear guidance and theoretical justification for optimizing the  
414 SWAT-C model. Furthermore, the proposed methodology exhibits strong generalizability and can be  
415 extended to module diagnosis and improvement in other coupled modeling systems.

#### 416 **4.3. Sources of DOC Prediction Biases**

417       Previous studies have generally indicated that the NSE values for daily DOC simulation using  
418 SWAT-C typically remain around 0.5 (Du et al., 2023; Mukundan et al., 2023; Qi et al., 2020a), even  
419 after extensive parameter calibration. This indicates that the limited performance observed in this study  
420 is more likely due to structural deficiencies in the model, even after good calibration. Therefore, the  
421 modular diagnostic framework proposed here aims not merely to improve model outputs, but also to  
422 identify and quantify structural bottlenecks that hinder the DOC simulation accuracy and inform future  
423 model refinement.

424       A combined analysis of SHAP global importance and residual contributions shows that DOC  
425 simulation errors mainly originate from the carbon module and its nonlinear interactions with  
426 meteorological and hydrological components. The vegetation module, particularly LAI, also introduces



427 significant errors due to its influence on carbon input and surface processes (Li et al., 2025a).

428 Among interaction terms, DOC-TEMIN underscores the importance of minimum temperature in  
 429 regulating carbon mineralization, while DOC-SOLAR and ET-SOLAR reflect the indirect effects of  
 430 radiation via soil heat and evapotranspiration (Slavik et al., 2023). DOC-WIND indicates that WIND  
 431 influences the transport of DOC mainly by inducing wind erosion, which alters surface conditions and  
 432 facilitates DOC mobilization (Guo et al., 2023). Although LAI shows modest global SHAP importance,  
 433 its high residual contribution reveals temporal or structural mismatches in the vegetation module. A  
 434 negative correlation between LAI and DOC output suggests that the model fails to capture seasonal  
 435 vegetation dynamics or carbon input variation (Gier et al., 2024; Li et al., 2025a), making LAI a latent  
 436 but important error source that requires improved temporal representation and coupling with carbon  
 437 processes. Moreover, climate warming has significantly altered vegetation phenology in recent decades,  
 438 leading to earlier start-of-season (SOS) and delayed end-of-season (EOS) trends (Fu et al., 2019; Geng  
 439 et al., 2020). These phenological shifts amplify the temporal complexity of LAI evolution, further  
 440 challenging the model's ability to simulate realistic canopy dynamics and accurately represent its  
 441 regulatory role in DOC production and transport. Other modules, such as pollutant transport and  
 442 precipitation input, demonstrated high global relevance but minimal residual impact, indicating reliable  
 443 structure and data quality. In contrast, relative humidity had low SHAP importance but substantial  
 444 residual contribution, likely due to indirect influences via evapotranspiration and soil moisture.

445 DOC simulation errors stem from complex, nonlinear interdependencies across modules. The  
 446 carbon and vegetation modules-especially LAI-are the dominant error sources, while meteorological  
 447 and hydrological variables contribute through both direct and indirect pathways. Refining the carbon  
 448 module and improving inter-module coupling are key to enhancing DOC simulation performance.

#### 449 **4.4. Significance and Future Perspectives of the SWAT-MDF Framework**

450 Accurately simulating and understanding the dynamics of DOC in data-scarce watersheds under  
 451 continuous environmental change remains a critical yet challenging task (Li et al., 2025b). This study  
 452 developed the SWAT-MDF diagnostic framework, which integrates the process-based SWAT-C model,  
 453 a data-driven learning module implemented through ML algorithms, and SHAP- and residual-based



454 interpretation to enhance the transparency and reliability of DOC simulations. By combining the  
455 physically based process mechanisms of SWAT-C model with the nonlinear learning capacity of ML,  
456 the framework effectively represents DOC variability under complex hydrological and environmental  
457 conditions. In addition, the integrated SHAP and residual analysis system provides interpretable  
458 insights into variable importance and sources of structural uncertainty.

459 More importantly, the SWAT-MDF diagnostic framework integrating SHAP and residual analysis  
460 offers a systematic and quantitative diagnostic tool for model error identification. This framework not  
461 only detects performance bottlenecks in SWAT-C model for DOC simulation but also exhibits strong  
462 generalizability, making it applicable to module diagnosis across other hydrological and  
463 biogeochemical processes. As such, it provides both a theoretical foundation and a practical pathway  
464 for structural improvement of process-based models that is applicable across regions and  
465 environmental conditions. In principle, the proposed diagnosis strategy is not restricted to SWAT-C and  
466 has the potential to be transferred to other models, such as SWAT+. Although SWAT+ represents the  
467 newest version of the SWAT family, carbon-related functionalities comparable to SWAT-C are still  
468 under development. In this context, the SWAT-MDF framework could serve as a transferable diagnostic  
469 reference to help identify model weaknesses and guide process improvement during the development  
470 and validation of future SWAT+ carbon modules. This also suggests that the framework can be  
471 extended to other models when needed. However, since the primary objective of this study is to  
472 diagnose and improve DOC simulations, we adopted the established SWAT-C model as the  
473 process-based backbone.

474 Despite these contributions, limitations remain. While SHAP and residual analysis are effective  
475 for identifying critical modules and influential variables, they serve primarily as diagnostic tools. They  
476 do not directly modify model structures or parameterization schemes. Substantive model improvement  
477 still requires the integration of experimental observations, long-term monitoring data, and theoretical  
478 insight to refine key processes and complete the cycle from error identification to resolution.

479 Future research should focus on: (1) incorporating anthropogenic activity datasets into the modeling  
480 framework to improve its responsiveness to real-world environmental changes; (2) using the current  
481 DOC module diagnosis system to guide field-based experiments and mechanistic investigations,



482 thereby supporting structural improvements of the SWAT-C model DOC simulation modules; (3)  
483 extending the proposed diagnosis strategy to other key hydrological and ecological variables, and  
484 developing standardized criteria for module diagnosis and cross-watershed model comparison.

## 485 5. Conclusion

486 In this study, we developed a SWAT-MDF coupled modeling framework that integrates the  
487 strengths of a process-based hydrological model and a data-driven deep learning model to simulate and  
488 diagnose daily-scale DOC dynamics in the Yalong River Basin. SHAP interpretation and residual  
489 analysis were incorporated to conduct a comprehensive diagnosis of model components. The aim of  
490 this study was to identify and quantify the structural sources of uncertainty in DOC simulation under  
491 complex and data-scarce conditions, thereby supporting targeted refinement of the SWAT-C model. Our  
492 main findings can be summarized as follows:

493 (1) Among the tested data-driven models, the Bi-LSTM-based SWAT-MDF configuration showed  
494 the most reliable performance (training  $NSE = 0.76$ ,  $KGE = 0.80$ ; testing  $NSE = 0.48$ ,  $KGE = 0.67$ ),  
495 confirming the advantage of combining process-based features with data-driven learning. However, the  
496 testing performance remained limited, indicating that structural deficiencies in SWAT-C continue to  
497 constrain DOC simulation and require further structural improvement.

498 (2) SHAP-based global interpretation identified DOC\_Simulate, TOT\_P, and PRE as dominant  
499 predictors of DOC, highlighting the strong interactions among carbon cycling, pollutant transport, and  
500 hydrological processes in the watershed.

501 (3) Residual analysis revealed that LAI, RH, and DOC\_Simulate were the most significant  
502 contributors to prediction errors, corresponding to the vegetation growth module, relative humidity  
503 input, and carbon module, respectively. These results suggest that these components currently represent  
504 performance bottlenecks and should be prioritized in future model optimization.

505 (4) By integrating SHAP and residual analysis, this study established a systematic module  
506 diagnosis framework. The results indicate that rainfall inputs and the pollutant module perform  
507 relatively well in DOC simulation, whereas the carbon module, vegetation growth module, and relative  
508 humidity inputs exhibit larger errors. These components represent key targets for improving the





509 accuracy and stability of future DOC simulations.

510



511 *Data availability.* The DOC dataset used in this study was obtained from the publication by Xu et al. (2024), titled  
512 Escalating carbon export from high-elevation rivers in a warming climate, published in Environmental Science &  
513 Technology. The data is available at: [https://doi.org/10.1021/acs.est.3c06777]. All analysis was conducted in  
514 Python. The Python code used in this study is available on Zenodo at [https://doi.org/10.5281/zenodo.16599142].

515

516 *Supplementary.* Supplementary materials are provided in Appendix A.

517

518 *Author contributions.* Zehong Huang: Methodology, Software, Formal analysis, Visualization, Writing-original  
519 draft. Shouzhi Chen: Data curation, Validation, Investigation, Writing-review & editing. Yufeng Gong: Resources,  
520 Data curation, Investigation. Zheng Wang: Validation, Writing-review & editing. Zheng Duan: Methodology,  
521 Validation, Writing-review & editing. Yongshuo Fu\*: Conceptualization, Supervision, Project administration,  
522 Funding acquisition, Writing-review & editing.

523

524 *Competing interest.* The authors declare that they have no known competing financial interests or personal  
525 relationships that could have appeared to influence the work reported in this paper.

526

527 *Disclaimer.* Publisher's note: Copernicus Publications remains neutral with regard to jurisdictional claims made in  
528 the text, published maps, institutional affiliations, or any other geographical representation in this paper. While  
529 Copernicus Publications makes every effort to include appropriate place names, the final responsibility lies with  
530 the authors.

531

532 *Acknowledgments.* The authors are grateful to the editor and reviewers for their valuable comments and  
533 suggestions, which have greatly helped us improve this paper.

534

535 *Financial support.* This study was supported by the Key Program of the National Natural Science Foundation of  
536 China (Grant 42430504), and the National Funds for Distinguished Young Youths (Grant 42025101), the Key  
537 Program of the National Natural Science Foundation of China (Grant 42330515), the Fundamental Research Funds  
538 for the Central Universities (2243300004) and the 111 Project (Grant B18006). We thank the reviewers and



539 associate editor of this manuscript for their valuable comments and suggestions that helped us to substantially  
 540 improve the paper.

## 541 **References**

542 Abbaspour, K., Vaghefi, S., and Srinivasan, R.: A guideline for successful calibration and  
 543 uncertainty analysis for soil and water assessment: a review of papers from the 2016 international  
 544 SWAT conference, *Water*, 10, 6, <https://doi.org/10.3390/w10010006>, 2017.

545 Azzam, A., Zhang, W., Akhtar, F., Shaheen, Z., and Elbeltagi, A.: Estimation of green and blue  
 546 water evapotranspiration using machine learning algorithms with limited meteorological data: A case  
 547 study in Amu Darya River Basin, Central Asia, *Comput. Electron. Agric.*, 202, 107403,  
 548 <https://doi.org/10.1016/j.compag.2022.107403>, 2022.

549 Carvalho, D. V., Pereira, E. M., and Cardoso, J. S.: Machine learning interpretability: a survey on  
 550 methods and metrics, *Electronics*, 8, 832, <https://doi.org/10.3390/electronics8080832>, 2019.

551 Cole, J. J., Prairie, Y. T., Caraco, N. F., McDowell, W. H., Tranvik, L. J., Striegl, R. G., Duarte, C.  
 552 M., Kortelainen, P., Downing, J. A., Middelburg, J. J., and Melack, J.: Plumbing the Global Carbon  
 553 Cycle: Integrating Inland Waters into the Terrestrial Carbon Budget, *Ecosystems*, 10, 172–185,  
 554 <https://doi.org/10.1007/s10021-006-9013-8>, 2007.

555 Ding, B., Yu, X., and Jia, G.: Exploring the controlling factors of watershed streamflow variability  
 556 using hydrological and machine learning models, *Water Resour. Res.*, 61,  
 557 <https://doi.org/10.1029/2024wr039734>, 2025.

558 Du, X., Zhang, X., Mukundan, R., Hoang, L., and Owens, E. M.: Integrating terrestrial and  
 559 aquatic processes toward watershed scale modeling of dissolved organic carbon fluxes, *Environ. Pollut.*,  
 560 249, 125–135, <https://doi.org/10.1016/j.envpol.2019.03.014>, 2019.

561 Du, X., Faramarzi, M., Qi, J., Lei, Q., and Liu, H.: Investigating hydrological transport pathways  
 562 of dissolved organic carbon in cold region watershed based on a watershed biogeochemical model,  
 563 *Environ. Pollut.*, 324, 121390, <https://doi.org/10.1016/j.envpol.2023.121390>, 2023.

564 Evans, C. D., Monteith, D. T., and Cooper, D. M.: Long-term increases in surface water dissolved  
 565 organic carbon: observations, possible causes and environmental impacts, *Environ. Pollut.*, 137, 55–71,



- 566 <https://doi.org/10.1016/j.envpol.2004.12.031>, 2005.
- 567 Fan, H., Jiang, M., Xu, L., Zhu, H., Cheng, J., and Jiang, J.: Comparison of Long Short Term  
 568 Memory Networks and the Hydrological Model in Runoff Simulation, *Water*, 12, 175,  
 569 <https://doi.org/10.3390/w12010175>, 2020.
- 570 Fu, Y. H., Piao, S., Delpierre, N., Hao, F., Hänninen, H., Geng, X., Peñuelas, J., Zhang, X.,  
 571 Janssens, I. A., and Campioli, M.: Nutrient availability alters the correlation between spring leaf-out  
 572 and autumn leaf senescence dates, *Tree Physiol.*, 39, 1277–1284,  
 573 <https://doi.org/10.1093/treephys/tpz041>, 2019.
- 574 Geng, X., Fu, Y. H., Hao, F., Zhou, X., Zhang, X., Yin, G., Vitasse, Y., Piao, S., Niu, K., De Boeck,  
 575 H. J., Menzel, A., and Peñuelas, J.: Climate warming increases spring phenological differences among  
 576 temperate trees, *Global Change Biol.*, 26, 5979–5987, <https://doi.org/10.1111/gcb.15301>, 2020.
- 577 Gier, B. K., Schlund, M., Friedlingstein, P., Jones, C. D., Jones, C., Zaehle, S., and Eyring, V.:  
 578 Representation of the terrestrial carbon cycle in CMIP6, *Biogeosciences*, 21, 5321–5360,  
 579 <https://doi.org/10.5194/bg-21-5321-2024>, 2024.
- 580 Grusson, Y., Sun, X., Gascoin, S., Sauvage, S., Raghavan, S., Anctil, F., and Sánchez-Pérez, J.-M.:  
 581 Assessing the capability of the SWAT model to simulate snow, snow melt and streamflow dynamics  
 582 over an alpine watershed, *J. Hydrol.*, 531, 574–588, <https://doi.org/10.1016/j.jhydrol.2015.10.070>,  
 583 2015.
- 584 Guo, Y., Ni, Z., Dong, Y., Wang, S., Wu, Y., Liu, S., and Huang, Y.: Overlooked great role of wind  
 585 erosion in terrestrial dissolved organic matter input to lake ecosystem in cold and arid regions, *Sci.*  
 586 *Total Environ.*, 890, 164272, <https://doi.org/10.1016/j.scitotenv.2023.164272>, 2023.
- 587 Guo, Z., Feng, C., Yang, L., and Liu, Q.: Bridging the gap: An interpretable coupled model  
 588 (SWAT-ELM-SHAP) for blue-green water simulation in data-scarce basins, *Agric. Water Manag.*, 306,  
 589 109157, <https://doi.org/10.1016/j.agwat.2024.109157>, 2024.
- 590 Hantush, M. M. and Kalin, L.: Stochastic residual-error analysis for estimating hydrologic model  
 591 predictive uncertainty, *J. Hydrol. Eng.*, 13, 585–596,  
 592 [https://doi.org/10.1061/\(ASCE\)1084-0699\(2008\)13:7\(585\)](https://doi.org/10.1061/(ASCE)1084-0699(2008)13:7(585)), 2008.
- 593 Harkort, L. and Duan, Z.: Estimation of dissolved organic carbon from inland waters at a large



594 scale using satellite data and machine learning methods, *Water Res.*, 229, 119478,  
 595 <https://doi.org/10.1016/j.watres.2022.119478>, 2023.

596 Hongyi Li, G. S. and Maddala: Bootstrapping time series models, *Econom. Rev.*, 15, 115–158,  
 597 <https://doi.org/10.1080/07474939608800344>, 1996.

598 Lawlor, A. J. and Tipping, E.: Metals in bulk deposition and surface waters at two upland  
 599 locations in northern England, *Environ. Pollut.*, 121, 153–167,  
 600 [https://doi.org/10.1016/S0269-7491\(02\)00228-2](https://doi.org/10.1016/S0269-7491(02)00228-2), 2003.

601 Lee, D., Karki, R., Kalin, L., Isik, S., Srivastava, P., and Zhang, X.: Management Strategies for  
 602 Dissolved Organic Carbon Reduction from Forested Watersheds using the SWAT-C model, *Environ.*  
 603 *Manag.*, 75, 1181–1200, <https://doi.org/10.1007/s00267-025-02128-y>, 2025.

604 Lee, J., Abbas, A., McCarty, G. W., Zhang, X., Lee, S., and Hwa Cho, K.: Estimation of base and  
 605 surface flow using deep neural networks and a hydrologic model in two watersheds of the Chesapeake  
 606 Bay, *Journal of Hydrology*, 617, 128916, <https://doi.org/10.1016/j.jhydrol.2022.128916>, 2023a.

607 Lee, J., Abbas, A., McCarty, G. W., Zhang, X., Lee, S., and Hwa Cho, K.: Estimation of base and  
 608 surface flow using deep neural networks and a hydrologic model in two watersheds of the Chesapeake  
 609 Bay, *J. Hydrol.*, 617, 128916, <https://doi.org/10.1016/j.jhydrol.2022.128916>, 2023b.

610 Li, M., Chen, S., Hao, F., Wang, N., Wu, Z., Xu, Y., Zhang, J., Zhang, Y., and Fu, Y. H.:  
 611 Integration of the vegetation phenology module improves ecohydrological simulation by the  
 612 SWAT-carbon model, *Hydrol. Earth Syst. Sci.*, 29, 2081–2095,  
 613 <https://doi.org/10.5194/hess-29-2081-2025>, 2025a.

614 Li, S.-L., Chetelat, B., Yue, F., Zhao, Z., and Liu, C.-Q.: Chemical weathering processes in the  
 615 Yalong River draining the eastern Tibetan Plateau, China, *J. Asian Earth Sci.*, 88, 74–84,  
 616 <https://doi.org/10.1016/j.jseaes.2014.03.011>, 2014.

617 Li, Y., Wang, G., Wang, W., Sun, X., Li, Y., Xiao, J., Xie, W., Ding, J., and Song, C.: Ultraviolet  
 618 radiation stimulates the degradability of groundwater-fed DOC during the baseflow period of streams  
 619 on the qinghai-tibet plateau permafrost region, *J. Hydrol.*, 653, 132751,  
 620 <https://doi.org/10.1016/j.jhydrol.2025.132751>, 2025b.

621 Liu, J., Liu, J., Du, X., Guo, R., Duan, Z., Yuan, B., and Liu, Y.: The importance of impoundment



interception in simulating riverine dissolved organic carbon, *Water Resour. Res.*, 60,  
<https://doi.org/10.1029/2024wr038133>, 2024.

Liu, X., Yang, M., Meng, X., Wen, F., and Sun, G.: Assessing the impact of reservoir parameters  
 on runoff in the yalong river basin using the SWAT model, *Water*, 11, 643,  
<https://doi.org/10.3390/w11040643>, 2019.

Lundberg, S. M., Erion, G., Chen, H., DeGrave, A., Prutkin, J. M., Nair, B., Katz, R., Himmelfarb,  
 J., Bansal, N., and Lee, S.-I.: From local explanations to global understanding with explainable AI for  
 trees, *Nat. Mach. Intell.*, 2, 56–67, <https://doi.org/10.1038/s42256-019-0138-9>, 2020.

Mosca, E., Szigeti, F., Tragianni, S., Gallagher, D., and Groh, G., 2022. SHAP-based explanation  
 methods: a review for NLP interpretability. *Proceedings of the 29th International Conference on*  
*Computational Linguistics*, pp. 4593–4603.

Mukundan, R., Gelda, R. K., Moknatie, M., Zhang, X., and Steenhuis, T. S.: Watershed scale  
 modeling of dissolved organic carbon export from variable source areas, *J. Hydrol.*, 625, 130052,  
<https://doi.org/10.1016/j.jhydrol.2023.130052>, 2023.

Pelletier, G. J., Chapra, S. C., and Tao, H.: QUAL2Kw – A framework for modeling water quality  
 in streams and rivers using a genetic algorithm for calibration, *Environ. Model. Softw.*, 21, 419–425,  
<https://doi.org/10.1016/j.envsoft.2005.07.002>, 2006.

Qi, J., Du, X., Zhang, X., Lee, S., Wu, Y., Deng, J., Moglen, G. E., Sadeghi, A. M., and McCarty,  
 G. W.: Modeling riverine dissolved and particulate organic carbon fluxes from two small watersheds in  
 the northeastern United States, *Environ. Model. Softw.*, 124, 104601,  
<https://doi.org/10.1016/j.envsoft.2019.104601>, 2020a.

Qi, J., Zhang, X., Yang, Q., Srinivasan, R., Arnold, J. G., Li, J., Waldhoff, S. T., and Cole, J.:  
 SWAT ungauged: Water quality modeling in the Upper Mississippi River Basin, *J. Hydrol.*, 584,  
 124601, <https://doi.org/10.1016/j.jhydrol.2020.124601>, 2020b.

Rathjens, H., Oppelt, N., Bosch, D. D., Arnold, J. G., and Volk, M.: Development of a grid-based  
 version of the SWAT landscape model, *Hydrol. Process.*, 29, 900–914,  
<https://doi.org/10.1002/hyp.10197>, 2015.

Razavi, T. and Coulibaly, P.: Streamflow Prediction in Ungauged Basins: Review of



650 Regionalization Methods, J. Hydrol. Eng., 18, 958–975,  
 651 [https://doi.org/10.1061/\(ASCE\)HE.1943-5584.0000690](https://doi.org/10.1061/(ASCE)HE.1943-5584.0000690), 2013.

652 Santos Nobre, J. and Da Motta Singer, J.: Residual Analysis for Linear Mixed Models, *Biom. J.*,  
 653 49, 863–875, <https://doi.org/10.1002/bimj.200610341>, 2007.

654 Siami-Namini, S., Tavakoli, N., and Namin, A. S.: The performance of LSTM and BiLSTM in  
 655 forecasting time series, in: 2019 IEEE International Conference on Big Data (Big Data), 2019 IEEE  
 656 International Conference on Big Data (Big Data), Los Angeles, CA, USA, 3285–3292,  
 657 <https://doi.org/10.1109/BigData47090.2019.9005997>, 2019.

658 Slavik, I., Kostrowski, D., and Uhl, W.: Effect of solar radiation on natural organic matter  
 659 composition in surface waters and resulting impacts on drinking water treatment, *Environ. Technol.*,  
 660 2023.

661 Srinivasan, R., Ramanarayanan, T. S., Arnold, J. G., and Bednarz, S. T.: LARGE AREA  
 662 HYDROLOGIC MODELING AND ASSESSMENT PART II: MODEL APPLICATION <sup>1</sup>, *JAWRA J.*  
 663 *Am. Water Resour. Assoc.*, 34, 91–101, <https://doi.org/10.1111/j.1752-1688.1998.tb05962.x>, 1998.

664 Tan, M. L., Gassman, P. W., Srinivasan, R., Arnold, J. G., and Yang, X.: A Review of SWAT  
 665 Studies in Southeast Asia: Applications, Challenges and Future Directions, *Water*, 11, 914,  
 666 <https://doi.org/10.3390/w11050914>, 2019.

667 Todini, E.: Hydrological catchment modelling: past, present and future, *Hydrology and Earth*  
 668 *System Sciences*, 11, 468–482, <https://doi.org/10.5194/hess-11-468-2007>, 2007.

669 Tyagi, K., Rane, C., Harshvardhan, and Manry, M.: Chapter 4 - regression analysis, in: *Artificial*  
 670 *Intelligence and Machine Learning for EDGE Computing*, edited by: Pandey, R., Khatri, S. K., Singh,  
 671 N. kumar, and Verma, P., Academic Press, 53–63,  
 672 <https://doi.org/10.1016/B978-0-12-824054-0.00007-1>, 2022.

673 Wang, K., Mukundan, R., Gelda, R. K., and Frei, A.: Modeling dissolved organic carbon export  
 674 from water supply catchments in the northeastern United States, *Sci. Total Environ.*, 963, 178532,  
 675 <https://doi.org/10.1016/j.scitotenv.2025.178532>, 2025.

676 Xu, S., Li, S.-L., Bufer, A., Klaus, M., Zhong, J., Wen, H., Chen, S., and Li, L.: Escalating carbon  
 677 export from high-elevation rivers in a warming climate, *Environ. Sci. Technol.*, 58, 7032–7044,



- 678 <https://doi.org/10.1021/acs.est.3c06777>, 2024.
- 679 Yang, Q. and Zhang, X.: Improving SWAT for simulating water and carbon fluxes of forest  
 680 ecosystems, *Sci. Total Environ.*, 569–570, 1478–1488, <https://doi.org/10.1016/j.scitotenv.2016.06.238>,  
 681 2016.
- 682 Yao, Z., Wang, Z., Wang, D., Wu, J., and Chen, L.: An ensemble CNN-LSTM and GRU adaptive  
 683 weighting model based improved sparrow search algorithm for predicting runoff using historical  
 684 meteorological and runoff data as input, *J. Hydrol.*, 625, 129977,  
 685 <https://doi.org/10.1016/j.jhydrol.2023.129977>, 2023.
- 686 Zhang, X., Izaurrealde, R. C., Arnold, J. G., Williams, J. R., and Srinivasan, R.: Modifying the Soil  
 687 and Water Assessment Tool to simulate cropland carbon flux: Model development and initial  
 688 evaluation, *Sci. Total Environ.*, 463–464, 810–822, <https://doi.org/10.1016/j.scitotenv.2013.06.056>,  
 689 2013.
- 690 Zhao, J., Zhang, N., Liu, Z., Zhang, Q., and Shang, C.: SWAT model applications: from  
 691 hydrological processes to ecosystem services, *Sci. Total Environ.*, 931, 172605,  
 692 <https://doi.org/10.1016/j.scitotenv.2024.172605>, 2024.
- 693 Zhao, Y., Dong, N., Li, Z., Zhang, W., Yang, M., and Wang, H.: Future precipitation, hydrology  
 694 and hydropower generation in the Yalong River Basin: Projections and analysis, *J. Hydrol.*, 602,  
 695 126738, <https://doi.org/10.1016/j.jhydrol.2021.126738>, 2021.
- 696 Zoremsanga, C. and Hussain, J.: Particle Swarm Optimized Deep Learning Models for Rainfall  
 697 Prediction: A Case Study in Aizawl, Mizoram, *IEEE Access*, 12, 57172–57184,  
 698 <https://doi.org/10.1109/ACCESS.2024.3390781>, 2024.
- 699